Biochemical Pharmacology 190 (2021) 114592

Contents lists available at ScienceDirect

Biochemical Pharmacology

journal homepage: www.elsevier.com/locate/biochempharm

UGT1A1 dysfunction increases liver burden and aggravates hepatocyte damage caused by long-term bilirubin metabolism disorder

Dan Liu [a,b], Qi Yu [a], Zibo Li [a], Lin Zhang [a], Ming Hu [a,c], Caiyan Wang [a,*], Zhongqiu Liu [a,*]

[a] Guangdong Key Laboratory for Translational Cancer Research of Chinese Medicine, Joint Laboratory for Translational Cancer Research of Chinese Medicine of the Ministry of Education of the People's Republic of China, International Institute for Translational Chinese Medicine, Guangzhou University of Chinese Medicine, Guangzhou, Guangdong 510006, China

[b] Affiliated Hospital of Integrated Traditional Chinese and Western Medicine, Nanjing University of Chinese Medicine, Nanjing, Jiangsu 210028, China

[c] Department of Pharmacological and Pharmaceutical Sciences, College of Pharmacy, University of Houston, Houston, TX 77030, United States

ARTICLE INFO

Keywords:
UGT1A1
Bilirubin
Gilbert's syndrome
Liver damage
Schisandrin B

ABSTRACT

UGT1A1 is the only enzyme that can metabolize bilirubin, and its encoding gene is frequently mutated. *UGT1A1*6* (G71R) is a common mutant in Asia which leads to the decrease of UGT1A1 activity and abnormal bilirubin metabolism. However, it is not clear whether low UGT1A1 activity-induced bilirubin metabolism disorder increases hepatocyte fragility. ugt1a$^{+/-}$ mice were used to simulate the *UGT1A1*6* (G71R) population. Under the same CCl_4 induction condition, ugt1a$^{+/-}$ mice showed severer liver damage and fibrosis, indicating that ugt1a1 dysfunction increased liver burden and aggravated hepatocyte damage. In the animal experiment with a continuous intraperitoneal injection of bilirubin, the ugt1a$^{+/-}$ mice livers had more serious unconjugated bilirubin accumulation. The accumulated bilirubin leads to hyperphosphorylation of IκB-α, Ikk-β, and p65 and a significant increase of inflammatory factor. The α-SMA and Collagen I proteins markedly up-regulated in the ugt1a$^{+/-}$ mice livers. Immunofluorescence and confocal microscopy showed that hepatic stellate cells and Kupffer cells were activated in ugt1a$^{+/-}$ mice. Comprehensive results show that there was a crosstalk relationship between low UGT1A1 activity-bilirubin-liver damage. Furthermore, cell experiments confirmed that unconjugated bilirubin activated the NF-κB pathway and induced DNA damage in hepatocytes, leading to the significant increase of inflammatory factors. UGT1A1 knockdown in hepatocytes aggravated the toxicity of unconjugated bilirubin. Conversely, overexpression of UGT1A1 had a protective effect on hepatocytes. Finally, Schisandrin B, an active ingredient with hepatoprotective effects, extracted from a traditional Chinese medicinal herb, which could protect the liver from bilirubin metabolism disorders caused by ugt1a1 deficiency by downregulating p65 phosphorylation, inhibiting Kupffer cells, reducing inflammation levels. Our data clarified the mechanism of liver vulnerability caused by cross-talk between low UGT1A1 activity bilirubin, and provided a reference for individualized prevention of liver fragility in Gilbert's syndrome.

1. Introduction

Hepatocellular carcinoma is a common malignant tumor worldwide [1]. More than 90% of liver cancers develop in chronically damaged tissues characterized by hepatocellular injury, inflammation, and fibrosis [2]. UGT1A1 is an important phase II metabolic enzyme and the only enzyme that can metabolize bilirubin [3,4]. Bilirubin is a toxic pigment produced by heme cell catabolism, and it is mainly detoxified in the liver [5]. A certain concentration of bilirubin can cause irreversible damage to the brain and nervous system [6]. However, the effects and

Abbreviations: UGT1A1, Human UDP Glucuronosyltransferase Family 1 Member A1; ugt1a1, mouse UDP Glucuronosyltransferase Family 1 Member A1; TCGA, the database of the Cancer Genome Atlas; LIHC, liver hepatocellular carcinoma; GS, Gilbert's syndrome; TKI, Tyrosine kinase inhibitor; WT, wild-type; ugt1a$^{-/-}$ mice, ugt1a1 gene knockout mice; ugt1a$^{+/-}$ mice, ugt1a1 gene knockdown mice; UCB, unconjugated bilirubin; CB, conjugated bilirubin; qPCR, quantitative polymerase chain reaction; PBS, phosphate-buffered saline; ALT, alanine aminotransferase; AST, aspartate aminotransferase; γ-GT, gamma-glutamyltransferase; PXR, pregnane X receptor; FBS, fetal bovine serum; BSA, Bovine serum albumin; UDPGA, uridine diphosphate glucuronic acid; OD, optical density; SEM, standard error of the mean; HLMs, human liver microsomes.

* Corresponding authors.
E-mail addresses: wangcaiyan@gzucm.edu.cn (C. Wang), liuzq@gzucm.edu.cn (Z. Liu).

https://doi.org/10.1016/j.bcp.2021.114592
Received 23 March 2021; Received in revised form 29 April 2021; Accepted 30 April 2021
Available online 4 May 2021

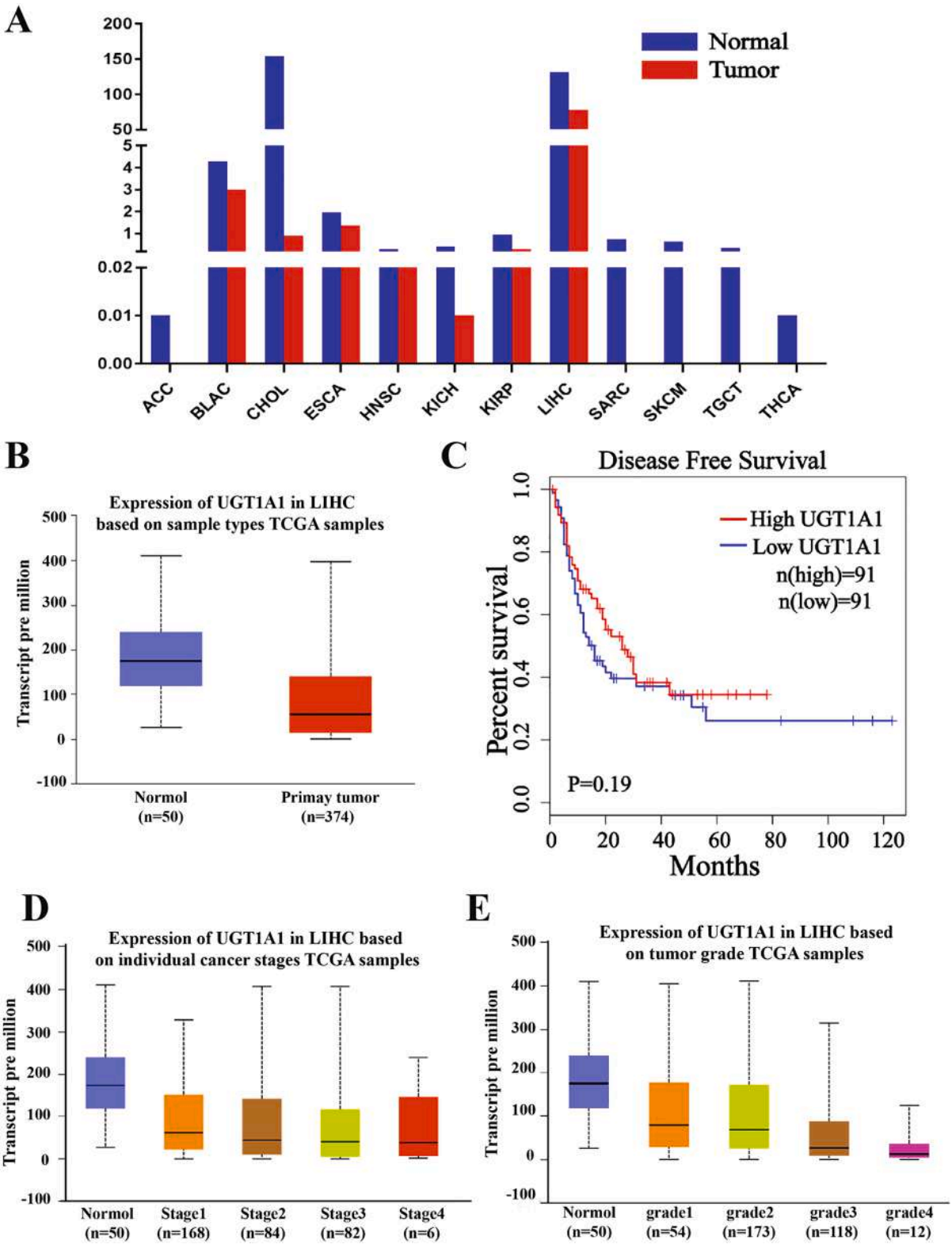

Fig. 1. UGT1A1 protein levels were significantly lower in the LIHC patients than in the normal group. (A) Comparison of UGT1A1 expression in different normal tissues and cancer tissues. (B) Comparison of UGT1A1 expression in normal tissues and Liver cancer tissue. (C) Survival curve analysis of liver cancer patients with different UGT1A1 levels. (D) Expression of UGT1A1 in LIHC at different cancer stages. (E) Expression of UGT1A1 in LIHC at different individual tumor stages.

mechanism of bilirubin accumulation in the liver on the progression of hepatic diseases remain largely unclear.

UGT1A1 polymorphism causes a decrease in enzyme activity, which is summarized in our previously published article [7]. To survey the relevance of UGT1A1 to liver disease, we analyzed the expression of UGT1A1 in normal people and liver cancer patients by the database of the Cancer Genome Atlas (TCGA). Analytical data showed that UGT1A1 level was significantly lower in the liver hepatocellular carcinoma (LIHC) patient than normal group (Fig. 1). Gilbert's syndrome (GS) is a well-known disorder of bilirubin metabolism. G71R mutant is highly

prevalent in the Asian population [8,9] and is a single-nucleotide polymorphism due to mutation of the glycine residue at position 71 to arginine. Tyrosine kinase inhibitor (TKI) drugs are targeted anticancer drugs. However, TKI treatment in GS increases the risk of liver damage and hyperbilirubinemia, which is closely related to low UGT1A1 activity [10]. If GS individuals have diseases or bad habits (smoking, alcohol use, or exposure to UGT1A1 inhibitors) that may lead to substantial and long-term accumulation of bilirubin in the liver. The elevated bilirubin may more easily exacerbate liver injury progression, although this is unknown.

Normal adults produce approximately 250 to 350 mg of bilirubin daily. *In vivo*, UCB is transported into liver cells by organic anion transporters (OATP1B1/1B3) and metabolized by UGT1A1 into conjugated bilirubin (CB). Finally, CB is excreted into the bile and blood circulation through an efflux transporter [11]. Current research points out that UCB is considered a potent antioxidant when present at moderate levels [12]. However, metabolic block of high bilirubin concentration can cause neurotoxicity [13,14] and liver toxicity [15,16]. Moreover, high levels of UCB are commonly seen in patients with liver disease [17]. However, a few data available on the toxic mechanism of bilirubin on hepatocytes.

Schisandrin B is isolated from the fruit of *Schisandra chinensis*, which is a well-known hepatoprotective traditional Chinese herb. Studies reported that the hepatoprotective effect of Schisandrin B is related to the activation of the pregnane X receptor (PXR) pathway, and promotion of liver regeneration [18,19], and induced expression of several core cell cycle proteins [20,21], and inhibition of TGF-β1-mediated NF-κB activation [22]. However, does Schisandrin B also have a hepatoprotective effect on UGT1A1 deficiency?

Here, studies have shown that bilirubin stasis induced the increase of phosphorylation of IκB-α, Ikk-β, and p65 and activated the NF-κB pathway in mice liver. This phenomenon was more pronounced in ugt1a1 gene knockdown mice (ugt1a$^{+/-}$ mice). The inflammatory factors and the liver fibrosis marker α-SMA and Collagen I were significantly increased in ugt1a$^{+/-}$ mice. The cell experiment showed UCB had an inhibitory effect on hepatocyte repair and proliferation and caused DNA damage in hepatocytes. Collectively, our data reveal a previously unappreciated role for UGT1A1 in hepatocellular injury pathogenesis. UGT1A1 dysfunction increases the liver burden and aggravates hepatocyte damage caused by long-term bilirubin metabolism disorder. Finally, we proved that Schisandrin B can protect not only Wild-type (WT) mice but also ugt1A1-deficient mice against liver damage.

2. Materials and methods

2.1. Animal studies and ethics statements

WT and ugt1a$^{+/-}$ male mice, weighing 18–22 g, were obtained from the Jackson Laboratory, USA. All mice were housed at 25 ± 1 °C at a humidity of 55 ± 10% and on a 12 h L/12 h D cycle (lights on 8:00 AM to 8:00 PM) with access to food and water in an SPF animal laboratory (Guangzhou University of Traditional Chinese Medicine, Guangzhou, China). All mice were on a C57BL/6 genetic background. All experiments were conducted according to the Guide for the Care and Use of Laboratory Animals of the China National Institutes of Health and were approved by the Institutional Animal Care and Use Committee (IACUC) of Guangzhou University of Traditional Chinese Medicine (approval number 2020R0002).

2.2. Animal administration

WT and ugt1a$^{+/-}$ mice were intraperitoneally injected with CCl_4 (300 μl/kg, Macklin, China) three times a week [23]. Four weeks later, a subset of ugt1a$^{+/-}$ mice were fed free 15% ethanol. Mice were sacrificed 24 h after the last dose in the ninth week. In another set of experiments, WT and ugt1a$^{+/-}$ mice were injected with bilirubin (i.p., 100 mg/kg, Herbest Biotechnology, China) once daily for 12 days. Solutol® HS15 (GLPBIO, USA), a commonly used non-toxic injection solubilizer [24], was dissolved in physiological saline at 10% w/v and warmed to 37 °C until dissolved. The obtained 10% (w/v) Solutol® HS15 was used to prepare 10 mg/mL bilirubin. The control group is a solvent group without bilirubin. Schisandirin B administration : Schisandirin B (Nanjing Jingzhu Biological Technology, China) was suspended in 0.5% (w/v) sodium carboxymethyl cellulose (CMC-Na, St. Louis, MO, USA) solution described previously [20]. Mice were administered with Schisandirin B (100 mg/kg) by gavage with an interval of 12 h. Plasma samples and liver tissue samples were collected for further experimental analysis.

Table 1
Sequences of all primers analyzed by real-time PCR.

Gene	Forward (5′ → 3′)	Reverse (5′ → 3′)
ugt1a1	GTCATCCAAAGACTCGGGCA	GACATTCAGGGTCACCCCAG
TNF-α	TGCTTGTGTCTGTCTTGCGT	CCCGTGAATCCACCATGTCT
IL-1β	TGCCACCTTTTGACAGTGATG	TGTGCTGCTGCGAGATTTGA
IL-6	TCCTTCCTACCCCAATTTCCA	GCACTAGGTTTGCCGAGTAGA
α-SMA	AGGGAGTAATGGTTGGAATGG	GGTGATGATGGCGTGTTCTAT
GAPDH	GGAGAAACCTGCCAAGTATGA	CCTGTTGCTGTAGCCGTATT

2.3. UCB, CB and cytokine concentration measurement

Blood samples were collected from the eyelid, and fresh liver samples were collected. All samples were stored at −80 °C until ready for use. The liver tissue (10 mg) was placed in 1 ml of pH 7.4 phosphate-buffered saline (PBS), homogenized by a tissue grinding instrument, centrifuged at 3000 rpm/min for 20 min. And the supernatant was collected. UCB and CB were detected using ELISA kits according to the manufacturer's protocol, described previously [25]. Serum concentrations of TNF-α, IL-1β, and IL-6 levels of all mice were determined via ELISA. All ELISA kits were purchased from Meimian Biotechnology (Yancheng, Jiangsu, China). The histogram was processed by GraphPad Prism 8.0 software.

2.4. Quantitative polymerase chain reaction (qPCR)

Total RNA was extracted from liver or cell samples by TRIzol reagent (GLPBIO, USA). Reverse transcription was performed to obtain cDNA by using a kit (Thermo Fisher Scientific, USA). RNA levels were assessed in an ABI 7500 instrument using SYBR@ Master Mix and the following primers (Table 1). The relative mRNA levels were determined by the $2^{-\Delta\Delta CT}$ method with the GAPDH gene as the internal control.

2.5. Western blotting

All samples were lysed in RIPA buffer (Servicebio, China) containing 1% phenylmethanesulfonyl fluoride (Gentihold, China) and placed on ice for half an hour. Then, samples were centrifuged at 12,000 rpm for 15 min. The supernatants were collected and the total protein concentration was determined by the bicinchoninic acid method. Equal samples were subjected to 10% sodium dodecyl sulfate polyacrylamide gel electrophoresis and transferred onto polyvinylidene difluoride membranes (Millipore, USA). Then, membranes were blocked with 5% BSA for 1 h at room temperature, incubated with primary antibodies (specific for UGT1A1-Abcam, USA; α-SMA, IκB-α, Ikk-β, and p65-Servicebio, China; Collagen I, p-IκB-α, p-Ikk-β, p-p65 and γH2AX-Affinity Biosciences, USA; GAPDH and β-actin-Servicebio, China) overnight, and washed 3 times for 10 min with TBST. Membranes were incubated at room temperature for 1 h with secondary antibodies. Protein bands were visualized using an Omega Lum G imaging system (Aplegen) and quantified with densitometry using ImageJ software.

2.6. Histopathological analysis

Liver tissues were fixed with 4% paraformaldehyde (Servicebio, China), dehydrated, transparentized, embedded in paraffin, and sectioned. The paraffin sections were dewaxed, dehydrated through a gradient alcohol series, washed with PBS for 5 min, immersed in hematoxylin staining solution for 10 min, washed with water, and stained with H&E staining solution. The paraffin sections were dewaxed with xylene, dehydrated through a gradient ethanol series, stained with Masson staining solution, differentiated with 5% phosphotungstic acid (Servicebio, China), and soaked in aniline solution. Then, the stained sections were gradually dehydrated with ethanol and cleared with xylene. Masson staining was performed to visualize liver fibrosis and cirrhosis status.

2.7. Measurement of AST, ALT and γ-GT

After collection, blood was placed at room temperature for 2 h or overnight at 4 °C and was then centrifuged at 3000 rpm and 2–8 °C for 15 min. Then, we used an automatic biochemical analyzer to measure those levels of serum alanine aminotransferase (ALT), aspartate aminotransferase (AST), and gamma-glutamyltransferase (γ-GT) in a Chemray 240 instrument (Shenzhen Leidu Life Technology, China). All kits were purchased from Changchun Huili Biotechnology (Changchun, Jilin, China). The remaining samples were stored at −80 °C.

2.8. RNA sequencing

The livers of WT and ugt1a$^{-/-}$ mice were collected in 3 days after birth. RNA was extracted through the TRIzol method, the purity and concentration were measured by a Nanodrop 2000 (Thermo Fisher Scientific, Wilmington, DE), and the integrity of the RNA was evaluated with an Agilent Bioanalyzer 2100 system (Agilent Technologies, CA, USA). RNA samples with RNA integrity number > 7.5 and a total amount > 1 μg were used for RNA library construction. We used a NEBNext® Ultra™ II RNA Library Prep Kit for Illumina (NEB, USA) to construct the RNA library. After the library was constructed, a Qubit®3.0 fluorometer (Life Technologies, CA, USA) was used for preliminary quantification, and the Agilent 2100 system then was used to detect the inserts in the library. After the size of the inserts met the requirements, qPCR was used to analyze the library. The effective concentration was accurately quantified to ensure the quality of the library. After the library was qualified, the qualified library was sequenced on the Illumina NovaSeq 6000 platform (Tsingke, Beijing, China).

2.9. Immunofluorescence

Paraffin sections of liver tissue were prepared by the same protocol for H&E staining. Sections were sequentially immersed in xylene, absolute ethanol, 85% alcohol, 75% alcohol, and distilled water for dewaxing. The microwave method was used for antigen retrieval. Then, the slides washed out in PBS. An autofluorescence quencher was added for 5 min and rinsed with water for 10 min. Slides were placed in 5% BSA solution, blocked for 30 min and incubated with the primary antibody (α-SMA-Servicebio, China; F4/80, CD68 and CD11b-Affinity Biosciences, USA) overnight at 4 °C. Then, the corresponding secondary antibody was added dropwise to the glass slides, and the tissue was incubated in the dark at room temperature for 50 min. Then, nuclei were counterstained with DAPI (Solarbio, china). Finally, the slides were mounted with an anti-fluorescence quenching mountant. Confocal images were acquired with a Pannoramic MIDI scanner, and images were acquired by the built-in software CaseViewer 2.3.

Table 2
Sequences of SiRNA.

Gene	Sense (5′ → 3′)	Antisense (5′ → 3′)
Si-1	GGAUCAAUGGUCUCAGAAATT	UUUCUGAGACCAUUGAUCCTT
Si-2	CCUUGGACGUGAUUGGUUUTT	AAACCAAUCACGUCCAAGGAA
Si-3	CCACAAAUCCAAGACCCAUTT	AUGGGUCUUGGAUUUGUGGTT

2.10. Immunohistochemistry

After the liver tissue sections are deparaffinized, hydrated, antigen retrieval, and blocked with 5% BSA, the primary antibody is incubated overnight at 4 °C. The tissue sections are washed 2–3 times with PBS, and then incubated with horseradish peroxidase-labeled secondary antibody for 1 h at room temperature. Then, the sections were washed with PBS and incubated with streptavidin-peroxidase for 1 h. Finally, the slices were developed with DAB and photographed with a microscope (Leica ICC50, Germany).

2.11. Cell culture and MTT assay

WRL68 was purchased from the Cell Resource Center of Shanghai Institutes for Biological Sciences, Shanghai EK-Bioscience Biotechnology. Cells were cultured at 37 °C in an incubator with 5% CO_2 in MEM supplemented with 10% fetal bovine serum (FBS, GIBCO, USA). Cells in logarithmic phase were trypsinized to prepare a cell suspension. Cells were counted with a countstar instrument and plated (100 μl) in each well of a 96-well culture plate. UCB solution was prepared according to the previously reported [26]. 5.84 mg of UCB was dissolved in 2 ml of 0.05 M sodium hydroxide solution, then 2 ml of 10% bovine serum albumin (BSA, GLPBIO, USA) was added and mixed well. Finally, the prepared UCB solution was filtered and sterilized by a 0.22 μM filter. The whole experiment operation needs to be protected from light. The edge wells of the 96-well culture plate were filled with sterile PBS. At a confluence of 50–70%, medium containing bilirubin at concentrations of 25, 50, 100, and 200 μM or vehicle was added. The UCB concentration of cell administration refers to the previous report [27]. Then, the pretreated cells were incubated with 10 μl of MTT reagent per well for 4 h, and the optical density (OD) was measured at a wavelength of 490 nm using a SPECTRA MAX 190 microplate reader (Molecular Devices, USA). The cell viability (%) was calculated as OD_{490} value in the experimental group/OD490 value in the control group × 100%.

2.12. Analysis of hepatocyte morphological changes

Cells were treated with bilirubin at concentrations of 25, 50, 100 and 200 μM or with vehicle. Then, cells were cultured at 37 °C in 5% CO_2 for 12 h. Untreated and bilirubin-treated WRL68 cells were examined for morphological changes by light microscopy (Leica DM500, Switzerland). To evaluate morphology, cells were harvested, transferred to cytospin slides, fixed with 75% ethanol for 1 min, and stained with H&E. Cells were photographed with a microscope.

2.13. Regeneration and proliferation of hepatocytes

EdU assay was performed as previously described [28]. In brief, the UCB concentrations were 50 and 100 μM. The same amount of solvent was added to the control group. Then, cells were cultured at 37 °C in 5% CO_2 for 12 h. Finally, cells were labeled with Hoechst 33342 and EdU. A fluorescence microscope was used for image analysis.

2.14. Small interfering RNA transfection

Log-phase WRL68 cells were trypsinized to prepare a cell suspension. Cells were counted with a Countstar instrument. After preparing the cell suspension, cells were plated (200 μl per well) in a 6-well culture plate. Transfection was performed when the cell confluence was 40–50%. Two tubes were prepared: 125 μl of Opti-MEM™ (GIBCO, USA) and 7.5 μl of Lipofectamine™ 3000 reagent (Invitrogen, USA) were added to one

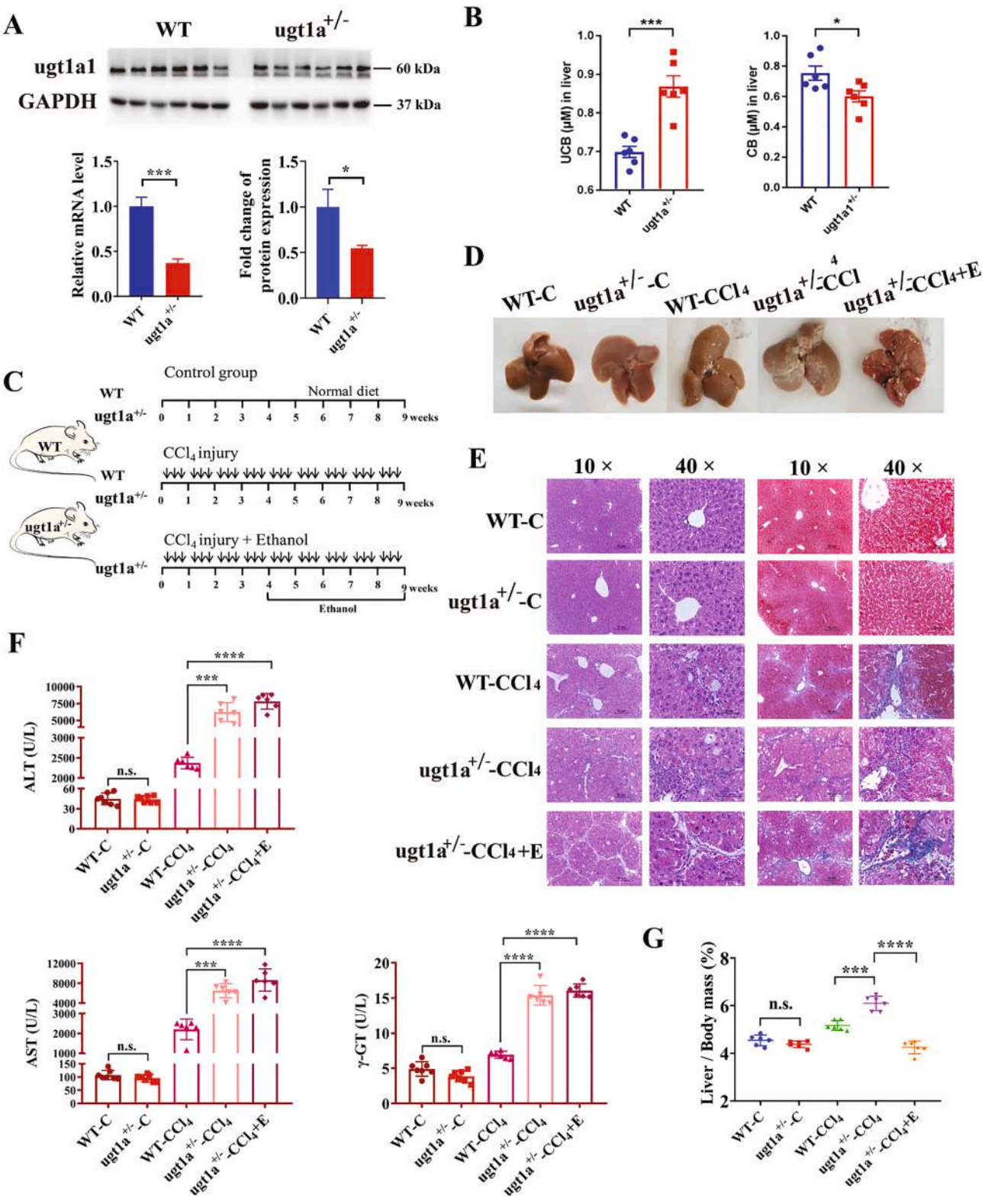

Fig. 2. Negative effects of ugt1a$^{+/-}$ mice on chronic liver injury. (A) The ugt1a1 protein and RNA expression in ugt1a$^{+/-}$ and WT mouse livers, as measured by western blotting and qPCR. In the lower left and right are statistical analysis of RNA relative expression and protein expression fold changes, respectively. (B) ELISA detection of UCB and CB in the liver and serum of ugt1a$^{+/-}$ and WT mice. (C) Timeline of the induction of chronic liver injury. The time point of intraperitoneal injection of CCL_4, three times a week. (D) The appearance of liver tissues in the different groups of mice. C-control, E-Ethanol. (E) H&E staining, (10 × Scale bar, 50 μm; 40×, Scale bar, 20 μm, left panel) and Masson staining (10 × Scale bar, 50 μm; 40×, Scale bar, 20 μm, right panel) of liver tissue of mice in different groups. (F) Determination of serum ALT, AST and γ-GT level in each group of mice. (G) Liver index statistics of mice in each group. Each group contained at least 6 mice. Statistical significance is shown as * ($p < 0.05$), ** ($p < 0.01$), *** ($p < 0.001$), **** ($p < 0.0001$).

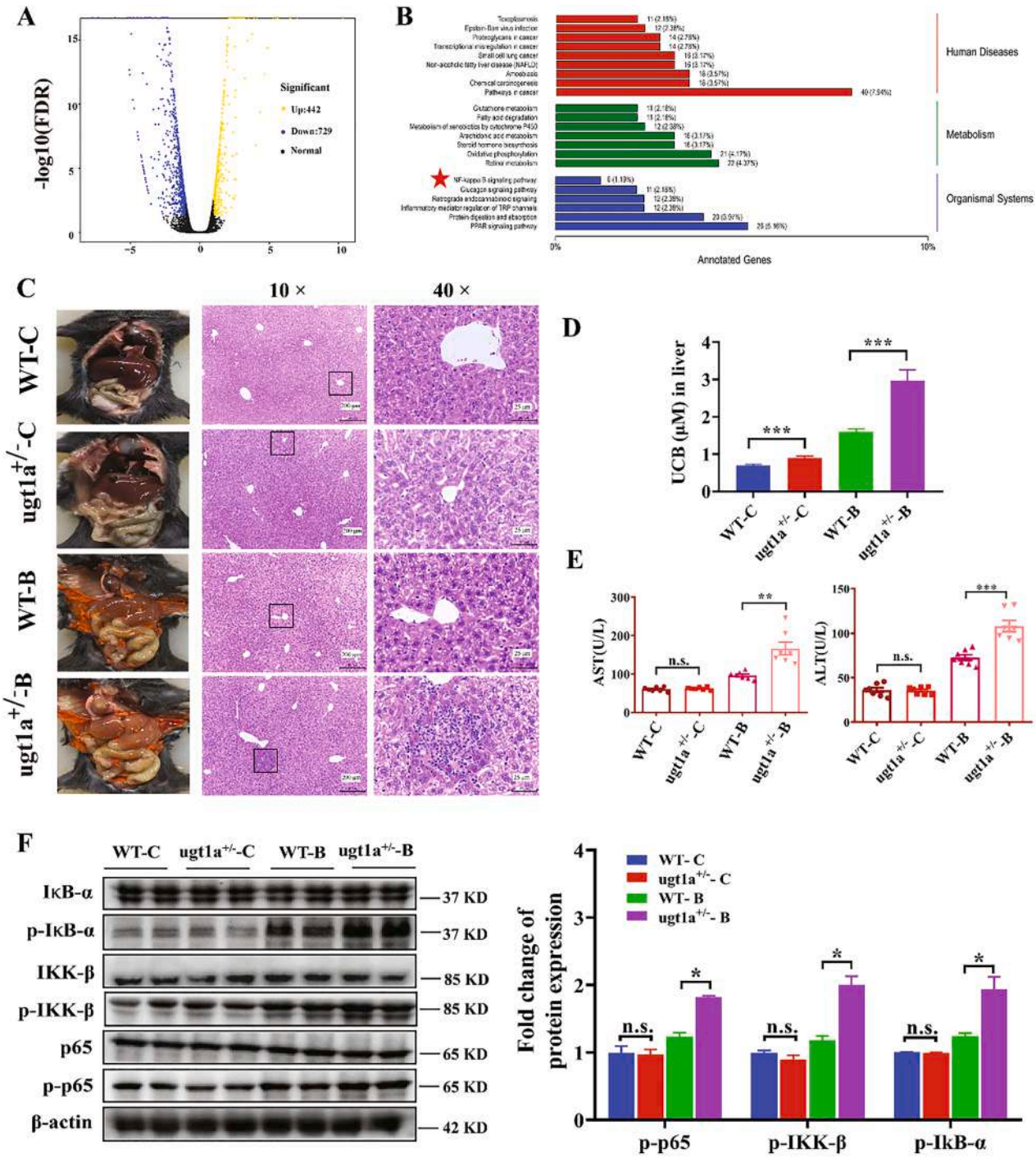

Fig. 3. Bilirubin-induced liver damage by activating the canonical NF-κB pathway in ugt1a1 deficiency. (A) Volcano plot showing differences in gene expression in the livers of WT and ugt1a$^{-/-}$ mice. Blue indicates high relative expression, yellow indicates low relative expression, and black indicates no significant difference. (B) KEGG pathway enrichment analysis. Different colors represent different related functions analysis. (C) The appearance and H&E staining of liver tissue after accumulation of bilirubin in mice. 10×, scale bar, 200 μm (left pane); 40×, scale bar, 25 μm (right panel). (D) The content of UCB in mice liver tissue. (E) The concentrations of ALT and AST in the serum of mice were measured. (F) Measurement of IκB-α, Ikk-β, p65, p-IκB-α, p-Ikk-β and p-p65 protein levels in mice livers by western blot (standardized by p65, Ikk-β, IκB-α, respectively). The right figure shows the significance of statistical analysis. Each group contained at least 6 mice. Statistical significance is shown as * ($p < 0.05$), ** ($p < 0.01$), *** ($p < 0.001$). (For interpretation of the references to color in this figure legend, the reader is referred to the web version of this article.)

tube, and 125 μl Opti-MEM™, 5 μg of siRNA and 10 μl of P3000™ reagent were added to the other tube. Then, the solutions in the two tubes were mixed well and incubated at room temperature for 15 min. Finally, they were added to the cell culture medium to be transfected into WRL68 cells. The small interfering RNA sequences are shown in Table 2.

2.15. Construction and transfection of recombinant UGT1A1-pCDNA3.1 and mutant G71R-pCDNA3.1 plasmid

The gene encoding UGT1A1 was amplified by PCR from cDNA from human 7721 cells. The gene sequence was cloned into the pCDNA3.1 vector. The G71R mutation was introduced by using a site-directed

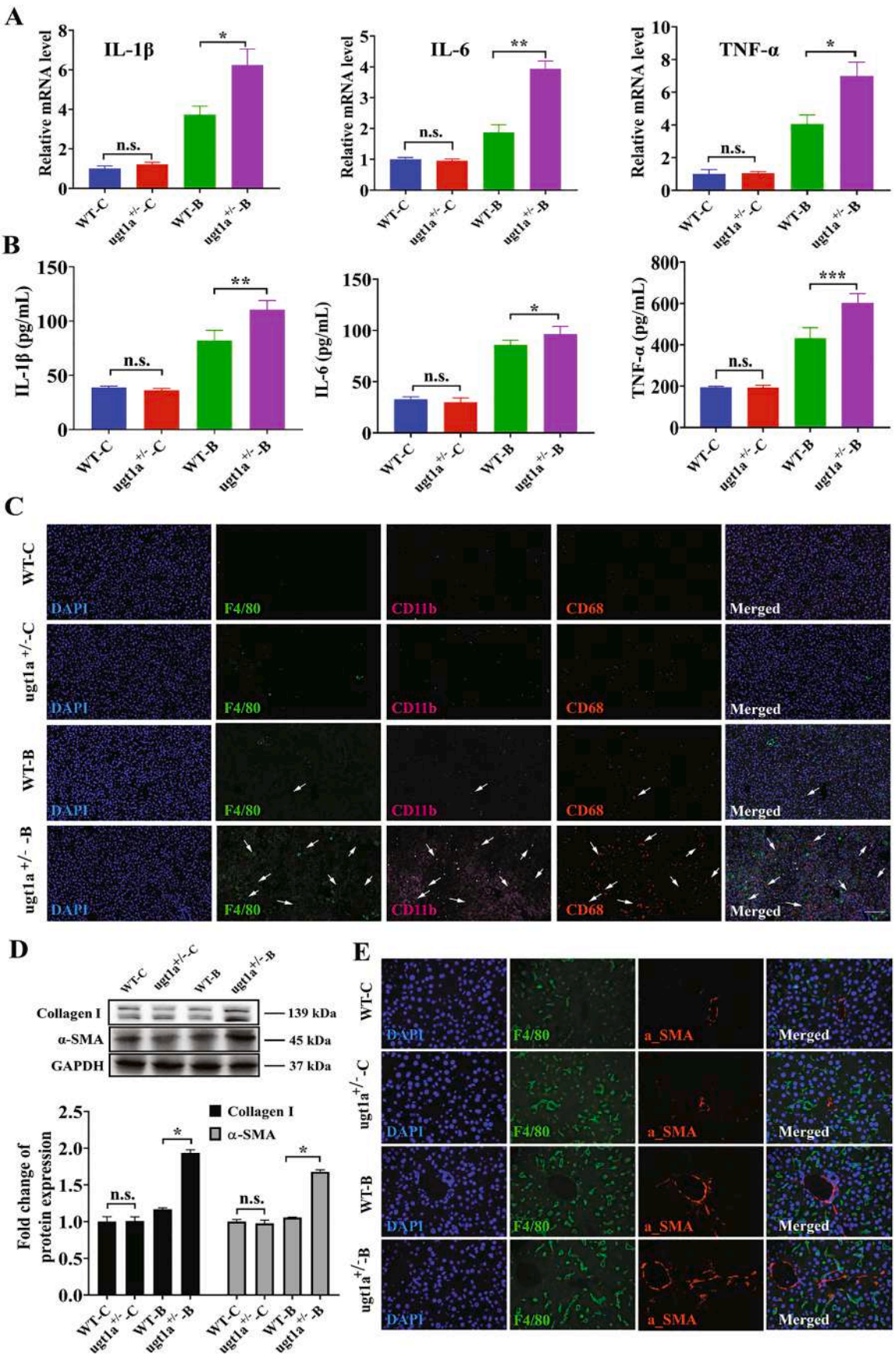

(caption on next page)

Fig. 4. Metabolic block of bilirubin activated Kupffer cells. (A) TNF-α, IL-6, and IL-β levels in the serum of ugt1a$^{+/-}$ and WT mice, as detected by ELISA kits. (B) Relative RNA expression levels of TNF-α, IL-6, and IL-β in ugt1a$^{+/-}$ and WT mice livers, as measured by qPCR. (C) High-magnification confocal images of ugt1a$^{+/-}$ and WT mouse liver tissue damaged by bilirubin, demonstrating that macrophages (Kupffer) identified by F4/80 (green), CD68 (red), and CD11b (pink) are activated (20×, scale bar, 50 μm). (D) Relative protein levels of α-SMA and collagen I in ugt1a$^{+/-}$ and WT mice livers, as measured by western blot (standardized by GADPH). (E) Immunohistochemical fluorescence in images of ugt1a$^{+/-}$ and WT mice liver tissue damaged by bilirubin, showing increased macrophage activity (green) and slight activation of α-SMA (red). 20×, scale bar, 25 μm. Each group contained at least 6 mice. Statistical significance is shown as * ($p < 0.05$), ** ($p < 0.01$), *** ($p < 0.001$). (For interpretation of the references to color in this figure legend, the reader is referred to the web version of this article.)

mutagenesis method with the following nucleotide substitution: 211G > A (G71R). WRL68 cells were seeded separately in 6-well plates. When the cell confluence was 60%, the cell culture medium was replaced with serum-free Opti-MEM™ (GIBCO, USA). The plasmid and Lipofectamine 3000 (Invitrogen, USA) were added to the medium at a ratio of 4 μg: 6 μl. After 12 h, the cell culture medium was replaced with a high-glycemic medium containing 10% fetal bovine serum without dual antibodies. After culture for 48 h, cells were harvested by scraping for subsequent experiments.

2.16. Molecular docking model of bilirubin and UGT1A1

The structure of UGT1A1 was obtained from the protein prediction database. ChemDraw 16.0 was used to draw the structures of bilirubin and UDPGA (uridine diphosphate glucuronic acid). All torsions of small molecules were checked, and gasteiger charges were assigned. Finally, AutoDock 4.2 software was used to generate the docking model of the UGT1A1 and bilirubin proteins. According to the docking integration principle, the docking model with the lowest energy value was selected.

2.17. Statistical analysis

Those data were analyzed with Student's *t* test or ANOVA to test the significance of differences between two groups. Unless otherwise stated, variations are indicated using the standard error of the mean (SEM) and expressed as mean ± SEM. Statistical significance is shown as * ($p < 0.05$), ** ($p < 0.01$), *** ($p < 0.001$), **** ($p < 0.0001$).

3. Results

3.1. The ugt1a1 deficiency aggravated liver damage in the process of simulating chronic liver injury

CCl_4 induced chronic liver injury leading to the accumulation of bilirubin metabolism has been reported in many studies [29–31]. To study the effect of UGT1A on the process of liver injury, we used the CCl_4 induced chronic liver injury model to simulate the process of liver damage. Firstly, the low expression of ugt1a1 in ugt1a$^{+/-}$ mice was verified. The ugt1a1 relative mRNA level and protein level in ugt1a$^{+/-}$ mice have decreased approximately by 50% compared with that in WT mice (Fig. 2A). The UCB in ugt1a$^{+/-}$ mice liver was obviously higher than that of WT mice (Fig. 2B). From the appearance of mouse liver tissue, the degree of liver cirrhosis was more severe in the ugt1a$^{+/-}$-CCl_4 group. And in the ugt1a$^{+/-}$-CCl_4-ethanol group, the liver was atrophied. The livers in the WT and ugt1a$^{+/}$-control groups were smooth and normal. The WT-CCl_4 group showed slight hyperplasia. However, the ugt1a$^{+/-}$-CCl_4 group had severe hyperplasia, with a tendency toward cirrhosis, and the capsule was uneven. The ugt1a$^{+/-}$-CCl_4- ethanol group showed severe atrophy (Fig. 2D). Histological analysis showed that the characteristics of the livers in the WT- and ugt1a$^{+/-}$-control groups were similar and that the cells were neatly arranged. The hepatocytes in the WT^{-}CCl_4 group and ugt1a$^{+/-}$-CCl_4 group were not distributed in a trabecular pattern, but were clustered. And each lesion had a surrounding inflammatory ring. The phenotypes in the ugt1a$^{+/-}$-CCl_4 and ugt1a$^{+/-}$-CCl_4-ethanol groups were even more disrupted (Fig. 2E). The Masson staining results verified the same patterns (Fig. 2E). In the WT -CCl_4 and ugt1a$^{+/-}$-CCl_4 group, the structure of liver lobules comprising hepatocytes was disordered, the hepatic cord was congested, and the volume of hepatocytes was significantly increased. The fibrosis in the ugt1a$^{+/-}$-CCl_4 and ugt1a$^{+/-}$-CCl_4 ethanol groups were more severe than that in the other groups. In the liver injury model of CCl_4 single factor and CCl_4-ethanol dual factor mice, ugt1a$^{+/-}$ mice reduced the proportion of liver to body weight (Fig. 2G), and increased those levels of ALT, AST and γ-GT in serum, and aggravated degrees of liver inflammation and fibrosis in mice (Fig. 2F). The total weight of the mice had no significant difference. These results indicate that ugt1a deficiency contributes to liver damage and liver fibrosis.

3.2. The ugt1a1 deficiency accompanied by long-term massive bilirubin stasis leads to liver damage by activating Kupffer cells and hepatic stellate cells

The liver is the main organ for detoxification of bilirubin and other exogenous substances. UGT1A1 is the only metabolic enzyme that detoxifies bilirubin, so the lack of UGT1A will promote the process of liver damage. It is not clear that whether the metabolism of bilirubin is more likely to cause liver damage in the absence of UGT1A. Of note, the body color of the ugt1a1 gene knockout mice (ugt1a$^{-/-}$ mice) indicated jaundice. The RNA sequencing data showed that ugt1a$^{-/-}$ mice caused upregulation of 442 genes and downregulation of 729 genes (Fig. 3A). The correlation was divided into three major categories based on the RNA sequencing data combined with the possible pathways of chronic inflammation in liver injury. The NF-κB pathway was found to be a functionally different pathway shown in Fig. 3B. A large amount of literature also pointed out that the activation of NF-κB pathway is closely related to liver injury [32]. Therefore, the NF-κB-related pathways were selected for further research.

Long-term continuous injection of bilirubin in WT and ugt1a$^{+/-}$ mice increased UCB level in liver. The UCB level in ugt1a$^{+/-}$ mice livers increased approximately 2-fold (Fig. 3D). The AST and ALT levels in ugt1a$^{+/-}$ mice increased significantly by 1.9- and 1.45-fold, respectively, compared with those in WT mice (Fig. 3E). In addition, the appearance of liver tissues indicated bilirubin stasis, as shown in Fig. 3C. And the results showed that hepatocyte nuclei in ugt1a$^{+/-}$ mice had local inflammation and chemotactic egress (Fig. 3C). Those results indicated that the liver tissue of ugt1a$^{+/-}$ mice had a lower tolerance to bilirubin than that of WT mice. The relative mRNA and protein levels of IL-1β, IL-6, and TNF-α were markedly increased in ugt1a$^{+/-}$ mice (Fig. 4A-B). The α-SMA and Collagen I protein levels were also significantly increased (Fig. 4D), which may imply activation of hepatic stellate cells, a group of cells that can induce liver fibrosis [33–35]. F4/80 was initially used to label macrophages, and the immunofluorescence showed that the macrophage population was increased in ugt1a$^{+/-}$ mice livers and the intensity of red fluorescence-labeled α-SMA was increased (Fig. 4E). To confirm our hypothesis, we examined whether these effects were related to the activation of Kupffer cells. Kupffer cells were further labeled with F4/80, CD11b and CD68. It was observed under a confocal microscope that the labeled Kupffer cells in the liver slices of the ugt1a$^{+/-}$ mice group were indeed significantly higher than the control group (Fig. 4C). Therefore, the increase in inflammatory factors may be due to the activation of Kupffer cells. The western blotting results confirmed the intensified induction of IκB-α and Ikk-β phosphorylation in ugt1a$^{+/-}$ mice livers (Fig. 3F). In addition, p65 was also hyperphosphorylated after bilirubin intervention (Fig. 3F). These results suggest that bilirubin accumulation in ugt1a1-deficient mice livers activated Kupffer cells to release inflammatory factors, stimulated the NF-κB pathway and caused

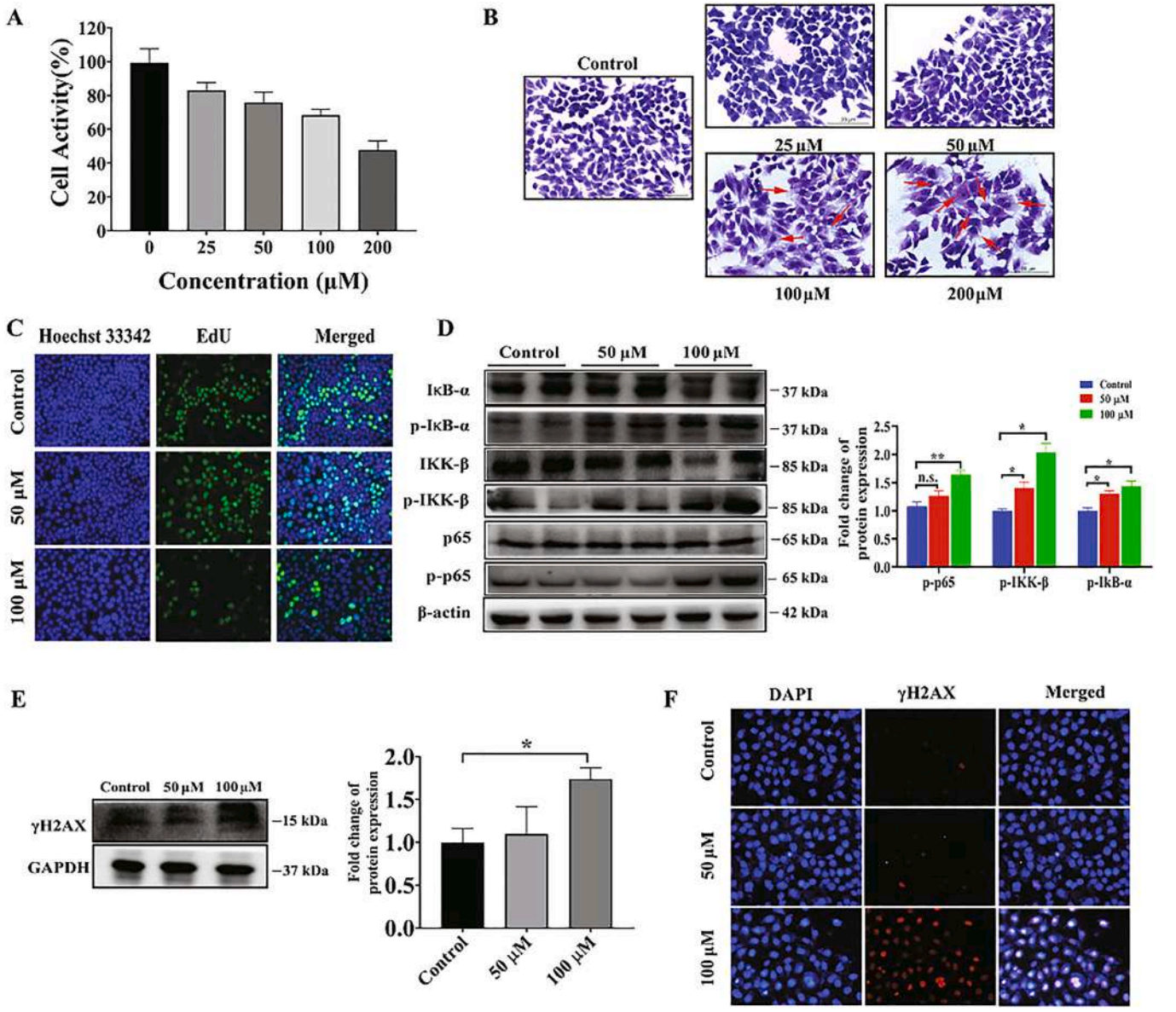

Fig. 5. Molecular mechanism of bilirubin-induced hepatocytes damage in cell. (A) MTT assay of bilirubin-treated WRL68 cells. (B) H&E staining of the effect of bilirubin on WRL68 cell morphology. 20×, scale bar, 20 μm. (C) The effect of bilirubin on the self-repair and proliferation of WRL68 cells, as detected by an EdU kit. 20×, scale bar, 25 μm. (D) Measurement of p65, p-p65, Ikk-β, p-Ikk-β, IκB-α, and p-IκB protein levels in WRL68 cells by western blotting (standardized by p65, Ikk-β, IκB-α, respectively). (E) γH2AX protein levels in WRL68 cells detected by western blotting (standardized GAPDH). (F) Immunofluorescence detection of γH2AX protein in WRL68 cells. At least 3 replicate samples were used for each experiment. Statistical significance is shown as * ($p < 0.05$), ** ($p < 0.01$).

liver damage. In addition, the increase of α-SMA expression indicated that hepatic stellate cells were activated. Therefore, compared with normal individuals, UGT1A1 deficiency has more fragile liver.

3.3. Bilirubin-induced p65 hyperphosphorylation and DNA damage led to hepatotoxicity

The neurotoxicity of bilirubin has been extensively studied. However, there are few studies on bilirubin-induced normal liver cell toxicity. To further determine the direct effect of bilirubin on hepatocytes, the bilirubin was added directly to the normal liver cells (WRL68). First, we observed the effects of bilirubin on WRL68 cells, including cell morphology, state, and viability. The results showed that low concentration bilirubin had little effect on WRL68 cells (Fig. 5A). However, when the bilirubin concentration was higher than 100 μM, WRL68 cells exhibited significant swelling (Fig. 5B). High concentration bilirubin (100 μM) inhibited hepatocyte proliferation. Further EdU experiment also confirmed that bilirubin (100 μM) inhibited the self-repair and regeneration ability of WRL68 cells (Fig. 5C). After bilirubin treatment, the phosphorylation levels of IκB-α, Ikk-β, and p65 in WRL68 cells were measured via western blotting (Fig. 5D). The results confirmed our hypothesis that the phosphorylation levels of IκB-α, Ikk-β, and p65 in the bilirubin-treated group were visibly increased, which indicated that the accumulation of bilirubin in the liver caused excessive protein phosphorylation, activating the NF-κB pathway. Repeated stimulation of external molecules, including oxidative stress, can damage cell macromolecules, especially DNA. For example, long-term alcohol abuse can cause hepatocyte DNA damage [36]. Therefore, after UCB was exposed to WRL68 cells, the expression of γH2AX increased significantly (Fig. 5E, F).

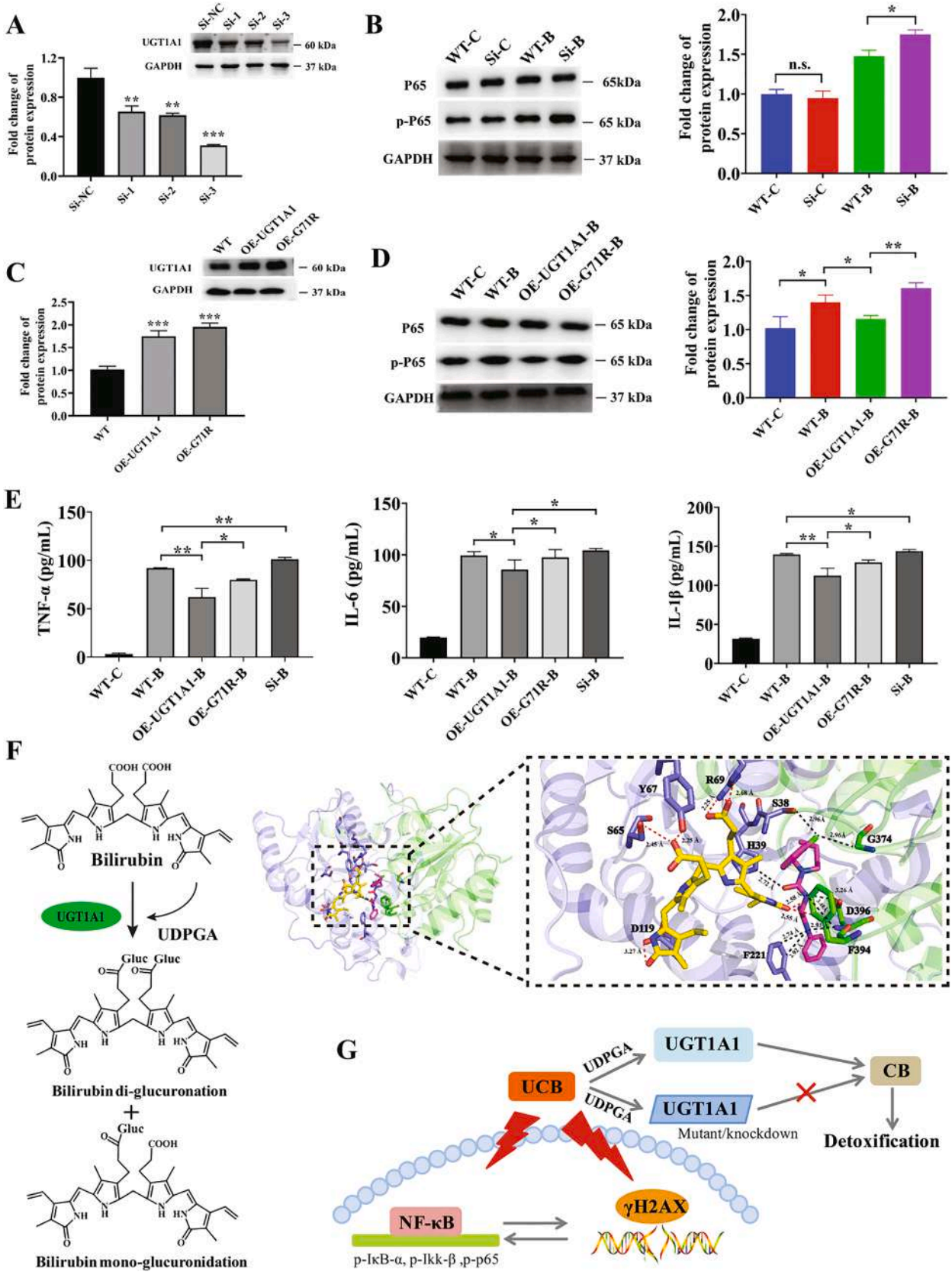

(caption on next page)

Fig. 6. The effect of UGT1A1 in hepatocytes on the bilirubin-induced injury. (A) UGT1A1 protein expression was silenced in WRL68 and small interfering RNA-3 cells in the subsequent UGT1A1 gene silencing experiment. (B) Western blot detection of p65 and p-p65. UGT1A1 silencing increased the phosphorylation of p65 in WRL68 cells. (C) UGT1A1 and GS-related mutant G71R were overexpressed in WRL68 cells, OE indicates overexpressed target protein. (D) Western blot detection of p65 and p-p65. (E) TNF-α, IL-6, and IL-β levels in WRL68 cells, as detected by ELISA kits. At least 3 replicate samples were used for each experiment. (F) Molecular docking of bilirubin and UGT1A1. The upper shows the schematic diagram of bilirubin glucuronidation. In the docking image, the yellow skeleton represents bilirubin, and the red skeleton represents cofactor UDPGA. The blue residues represent the N-terminal domain residues of UGT1A1, and the green residues represent the C-terminal domain residues of UGT1A1. The red dotted line represents the hydrogen bonding interaction between bilirubin and UGT1A1, and the black dotted line represents the hydrogen bonding interaction between UDPGA and UGT1A1 (Distance<3.5 Å). (G) Overview mechanism of UCB involvement in liver cell injury. Statistical significance is shown as * ($p < 0.05$), ** ($p < 0.01$), *** ($p < 0.001$). (For interpretation of the references to color in this figure legend, the reader is referred to the web version of this article.)

3.4. GS-related mutant UGT1A1 and knockdown UGT1A1 aggravate bilirubin-induced hepatocytes injury.

We then sought to explain the specific mechanism that low activity of UGT1A1 causes bilirubin accumulation to damage hepatocytes. The G71R mutation in UGT1A1 is a common low-activity mutant in the Asian population. We investigated the tolerance of hepatocytes against UCB toxicity after knocking down UGT1A1, overexpressing UGT1A1 and G71R, respectively. After silencing UGT1A1 in WRL68 cells, bilirubin treatment (100 μM) resulted in the increase of p65 phosphorylation and inflammatory factors (Fig. 6A,B). Conversely, UGT1A1 overexpression reduced the increase of inflammatory factors and p65 phosphorylation caused by bilirubin (Fig. 6C,D). Overexpression of GS-related mutant UGT1A1 (G71R) in WRL68 cells, the inflammatory factors and p65 phosphorylation were increased, comparing with the overexpression-UGT1A1 group (Fig. 6E). Collectively, those evidence suggested that hepatocytes with low UGT1A1 activity have decreased tolerance to bilirubin, which may lead to liver vulnerability.

Furthermore, we analyzed the effect of G71R mutation on the interaction between UDPGA and bilirubin from the perspective of protein and molecular interaction. The G71R mutation results in a longer side chain of 71st amino acid residue. When bilirubin reacted with UDPGA, longer side chains of residues caused steric hindrance by deflection, resulting in a decrease in the activity of the G71R mutant. Fig. 6F showed the UGT1A1 residues that bind bilirubin, including S65, Y67, and R69 located near G71. Bilirubin has two binding sites that can be glucuronated, as shown in Fig. 6F. It also indirectly indicates that the mutant protein may retain some activity because one of these sites is not affected by steric hindrance. In short, UGT1A1 dysfunction may lead to the accumulation of UCB. When a certain amount of UCB is exposed to liver cells, it stimulates the activation of the NF-κB pathway and induces DNA damage to cause liver cell damage (Fig. 6G).

3.5. The protective effect of Schisandrin B against liver damage caused by long-term bilirubin stasis induced by ugt1a1 deficiency

Schisandra has been widely used as a traditional herbal medicine to treat various diseases in many countries. Its main pharmacological functions include neuroprotection [37], immunity enhancement [38], and liver protection [39]. Schisandrin B is an active ingredient of Schisandra. ugt1a$^{+/-}$ mice and WT mice were intragastrically administered with Schisandrin B to prevent and treat liver damage caused by bilirubin stasis. The dosing regimen is shown in Fig. 7A. The control group was administered with the same solvent to eliminate interference. The appearance of liver tissue and the results of H&E staining proved that Schisandrin B had a certain hepatoprotective effect in WT and ugt1a$^{+/-}$ mice, as shown in Fig. 7B. The chemotaxis of hepatocytes and nuclei in Schisandrin B mice group were reduced. Schisandrin B treatment significantly reversed the serum ALT levels in ugt1a$^{+/-}$ and WT mice. The serum AST levels and the p65 phosphorylation in the ugt1a$^{+/-}$ and WT mice group with Schisandrin B treatment were also decreased (Fig. 7C,D). In addition, we further investigated whether Schisandrin B affects the activation of liver immune cells. The results showed that F4/80 infiltration and the significant increase of CD68 and CD11b occurred in ugt1a$^{+/-}$ mice liver tissue administered with bilirubin (Fig. 7E). This also confirmed our previous immunofluorescence results. Previous studies pointed out that Schisandrin B can inhibit oxidative stress by activating Nrf2 and nuclear receptor PXR to promote the expression of ugt1a1. We found that Schisandrin B can synergistically reduce inflammation by inhibiting the phosphorylation of p65 and the activation of Kuffer cells to protect the liver from damage (Fig. 7F). These comprehensive results confirmed that Schisandrin B can protect against liver damage in individuals with low ugt1a1 activity.

4. Discussion and conclusion

UGT1A1 has been widely studied in the field of drug metabolism for decades. In our previous studies, we have found that the activity of UGT1A1 in tumor-derived human liver microsomes (HLMs) was lower than that in adjacent normal HLMs, and the relative UGT1A1 protein and gene expression levels in tumor tissue were significantly reduced [40]. We speculated that UGT1A1 may be a dominant factor in liver damage progression. In this research, preliminary experiments showed that during the induction of chronic liver damage, the ugt1a$^{+/-}$ mice has more serious liver injury, indicating that the reduction of ugt1a aggravated the liver damage process.

UGT1A1 has been proven to be the only enzyme that can detoxify bilirubin. Liver damage is often accompanied by an increase in bilirubin, and it is unclear whether bilirubin will aggravate liver damage. Although Veel *et al.* reported that intravenous infusion of bilirubin can cause hepatocyte cytoplasmic vacuolation and tubule cholestasis [16]. The current research on bilirubin toxicity is focused on the neurological field. To further study the crosstalk relationship between low UGT1A1 activity, bilirubin and hepatocyte damage. WT and ugt1a$^{+/-}$ mice were intraperitoneally injected with bilirubin continuously. The ugt1a$^{+/-}$ mice liver showed more severe accumulation of UCB, indicating that ugt1a$^{+/-}$ mice had significantly lower bilirubin metabolic tolerance than WT mice. In this study, Kupffer cells were obviously activated in ugt1a$^{+/-}$ mice groups. Kupffer cells are phagocytic cells located on the inner surface of liver sinusoids, accounting for 80–90% of the macrophages colonized throughout the body. Once the liver is damaged, Kupffer cells will be activated and proliferated, accompanied by secretion of the cytokines TNF-α, IL-1β and IL-6 [41]. This may also partially explain why the levels of inflammatory factors in UGT1A1-deficient mice were higher than those in WT mice. In addition, the consistent result was obtained in the subsequent immunohistochemical staining experiment (shown in Fig. 8).

A research pointed out that the inflammatory cytokine TNF-α can promotes the long-term expansion of primary hepatocytes, which may also be a warning of liver fibrosis [42]. Herein, the levels of α-SMA and Collagen I were increased significantly in ugt1a$^{+/-}$ mice, indicating that hepatic stellate cells were also activated. These results proved that the accumulation of UCB in ugt1a$^{+/-}$ mice can stimulate Kupffer cells to release inflammatory factors, and further activated hepatic stellate cells. Under the stimulation of bilirubin, the IκB-α, Ikk-β and p65 in ugt1a$^{+/-}$ mice livers were hyperphosphorylated resulted in the activation of NF-κB. Furthermore, studies have reported that the activation of NF-κB can inhibit the expression of UGT1A1, thereby aggravating hyperbilirubinemia in the inflammatory process [43]. These two pathways may form a vicious circle with each other, exacerbating the disease of

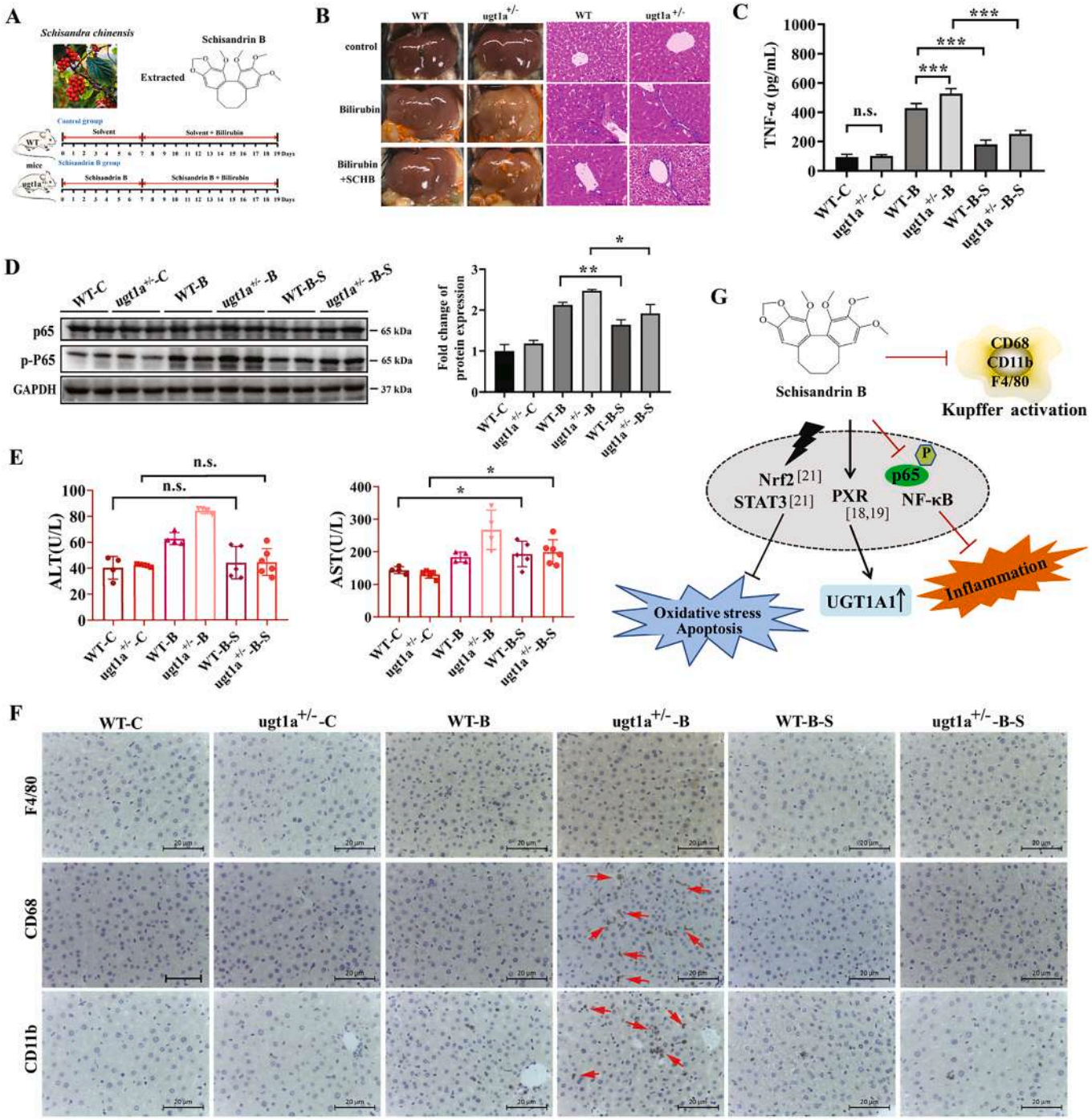

Fig. 7. Protective effect of Schisandrin B on bilirubin-induced liver injury in ugt1a1 deficiency (A) Photograph of a *Schisandra chinensis* plant and chemical structural formula of Schisandrin B (upper panel). Timeline of Schisandrin B and bilirubin administration. (B) Photograph and H&E staining of mice liver tissues treated with Schisandrin B. 40×, scale bar, 20 μm. S is short for Schisandrin B. (C) The concentration of TNF-α in the serum. (D) Measurement of p65 and p-p65 protein levels in the livers of ugt1a$^{+/-}$ and WT mice by western blotting. The right panel shows the statistical difference between the densities of the bands on the blots, as analyzed by *t* test. (E) The concentration of ALT and AST in the serum. (F) Immunohistochemical detection of F4/80, CD68 and CD11 protein expression in mice liver tissues. Scale bar, 20 μm. (G) Summary mechanism of Schisandrin B on bilirubin-induced liver injury in ugt1a1 deficiency. At least 4 mice per group were evaluated. Statistical significance is shown as * ($p < 0.05$), ** ($p < 0.01$), *** ($p < 0.001$).

the organism. Collectively, this evidence confirmed that ugt1a1 deficiency was more likely to cause liver damage than normal ugt1a1 activity mice.

In current studies, UCB-induced neuronal cytotoxicity is mainly related to oxidative stress [44,45], DNA damage [46,47], histone acetylation [48], proteasome inhibition [49]. Only two research literature reports on the effect of bilirubin in promoting the apoptosis and increasing reactive oxygen species of Hepa1c1c7 have been retrieved [50,51]. Little is known about the effect of UCB on normal and UGT1A1 knockdown / UGT1A1 mutate liver cells. In our cellular study, UGT1A1 knockdown increased vulnerability to liver damage based on bilirubin-induced protein hyperphosphorylation. It is widely recognized that increased oxidative stress could result in severe damage to cellular macromolecules, especially to DNA [46]. We found that 100 μM UCB

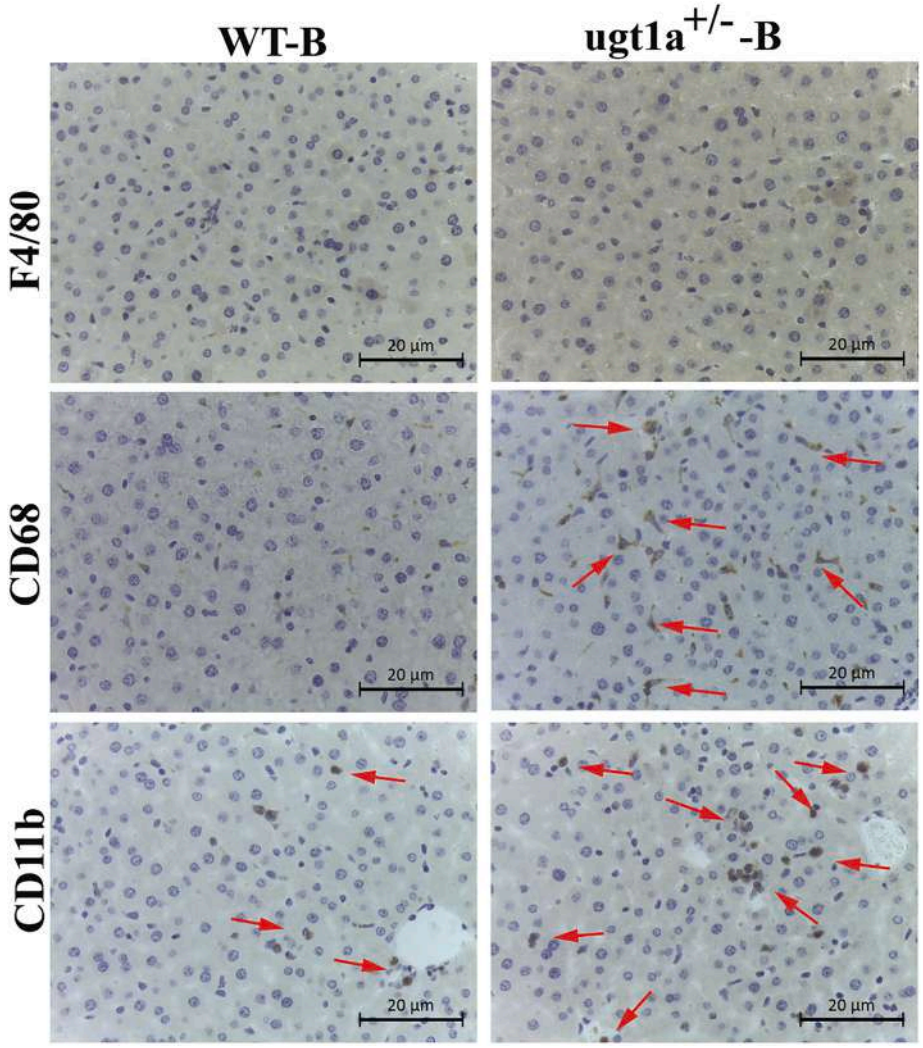

Fig. 8. The expression of F4/80, CD68 and CD11 proteins in liver tissues of WT and ugt1a$^{+/-}$ mice after intraperitoneal injection of bilirubin detected by immunohistochemistry.

can induce DNA damage in WRL68 cells by detecting γH2AX. In summary, Bilirubin-induced oxidative stress and DNA damage cause liver cell damage.

There is a hypothesis that the ugt1a1 expression could be increased by activating the PXR, CAR, FXR, and Nrf2 target genes in individuals with low expression of ugt1a1 [52], thereby combating liver injury. Current studies have shown that ginsenoside Rg1 [53], vitamin C [54], picroside II [55], carinoside [56] and Schisandrin B [18,19] can increase the protein level of UGT1A1 through the above mentioned pathways and exert hepatoprotective effects. And Schisandrin B can reverse the lithocholic acid-induced increase of serum bilirubin level by activating PXR to up-regulate UGT1A1 expression [57]. Therefore, we investigated the preventive and therapeutic effects of Schisandrin B on ugt1a$^{+/-}$ mice. In our study, the results confirmed that Schisandrin B can reduce liver damage caused by bilirubin accumulation in ugt1a$^{+/-}$ mice based on reducing the inflammatory response and inhibiting the activation of Kupffer cells and hepatic stellate cells. This is the first report to reveal the mechanism that UGT1A1 dysfunction may lead to hepatic vulnerability induced by the accumulation of bilirubin in the liver. The Schisandrin B prevention provides a personalized treatment to protect liver from fragility in UGT1A1 deficiency people.

Declaration of Competing Interest

The authors declare that they have no known competing financial interests or personal relationships that could have appeared to influence the work reported in this paper.

This work was supported by the fund of National Sciences Foundation of China (Nos. 81930114, 81720108033), The National Key Research and Development Program of the Ministry of Science and Technology of the People's Republic of China (No. 2017YFE0119900), The Lingnan Traditional Chinese Medicine Modernization Project (No. 2020B1111100004), Guangdong Key Laboratory for Translational Cancer Research of Chinese Medicine (No. 2018B030322011).

Author contributions

Dan Liu performed the experiments; Zhongqiu Liu and Caiyan Wang designed the project and revised the manuscript; Ming Hu provided experimental suggestions; Dan Liu, Qi Yu, Zibo Li and Lin Zhang performed the informatics analyses and experiments; Dan Liu wrote the paper.

References:

[1] J.D. Yang, P. Hainaut, G.J. Gores, A. Amadou, A. Plymoth, L.R. Roberts, A global view of hepatocellular carcinoma: trends, risk, prevention and management, Nat. Rev. Gastroenterol. Hepatol. 16 (2019) 589–604.

[2] Baglieri J, Brenner DA, Kisseleva T. The role of fibrosis and liver-associated fibroblasts in the pathogenesis of Hepatocellular Carcinoma. International journal of molecular sciences 2019;20.

[3] T. Iyanagi, Molecular mechanism of phase I and phase II drug-metabolizing enzymes: implications for detoxification, Int. Rev. Cytol. 260 (2007) 35–112.

[4] Piter J. Bosma JS, Bart Goldhoorn, Conny Bakker, and Ronald P. J. Oude Elferink. Bilirubin UDP-glucuronosyltransferase1 is the only relevant bilirubin glucuronidating Isoform in Man. The journal of biological chemistry 1994;269: 17960-4.

[5] M.F. Yueh, S. Chen, N. Nguyen, R.H. Tukey, Developmental, genetic, dietary, and xenobiotic influences on neonatal hyperbilirubinemia, Mol. Pharmacol. 91 (2017) 545–553.

[6] C. Mancuso, Bilirubin and brain: A pharmacological approach, Neuropharmacology 118 (2017) 113–123.

[7] D. Liu, L. Zhang, L.X. Duan, J.J. Wu, M. Hu, Z.Q. Liu, C.Y. Wang, Potential of herb-drug / herb interactions between substrates and inhibitors of UGTs derived from herbal medicines, Pharmacol. Res. 150 (2019), 104510.

[8] L. Cheng, M. Li, J. Hu, W. Ren, L. Xie, Z.P. Sun, B.R. Liu, G.X. Xu, X.L. Dong, X. P. Qian, *UGT1A1*6* polymorphisms are correlated with irinotecan-induced toxicity: a system review and meta-analysis in Asians, Cancer Chemother. Pharmacol. 73 (2014) 551–560.

[9] Y. Yang, M. Zhou, M. Hu, Y. Cui, Q. Zhong, L. Liang, F. Huang, *UGT1A1*6* and *UGT1A1*28* polymorphisms are correlated with irinotecan-induced toxicity: A meta-analysis, Asia-Pacific J. Clin. Oncol. 14 (2018) e479–e489.

[10] H. Qosa, B.R. Avaritt, N.R. Hartman, D.A. Volpe, *In vitro* UGT1A1 inhibition by tyrosine kinase inhibitors and association with drug-induced hyperbilirubinemia, Cancer Chemother. Pharmacol. 82 (2018) 795–802.

[11] J.H. Chang, E. Plise, J. Cheong, Q. Ho, M. Lin, Evaluating the in vitro inhibition of UGT1A1, OATP1B1, OATP1B3, MRP2, and BSEP in predicting drug-induced hyperbilirubinemia, Mol. Pharm. 10 (2013) 3067–3075.

[12] L. Vitek, Bilirubin as a signaling molecule, Med. Res. Rev. 40 (2020) 1335–1351.

[13] P. Karimzadeh, M. Fallahi, M. Kazemian, N. Taslimi Taleghani, S. Nouripour, M. Radfar, Bilirubin Induced Encephalopathy, Iran. J. Child Neurol. 14 (2020) 7–19.

[14] A.S. Falcao, A. Fernandes, M.A. Brito, R.F. Silva, D. Brites, Bilirubin-induced immunostimulant effects and toxicity vary with neural cell type and maturation state, Acta Neuropathol. 112 (2006) 95–105.

[15] A.A. Laskar, M.A. Khan, A.H. Rahmani, S. Fatima, H. Younus, Thymoquinone, an active constituent of Nigella sativa seeds, binds with bilirubin and protects mice from hyperbilirubinemia and cyclophosphamide-induced hepatotoxicity, Biochimie 127 (2016) 205–213.

[16] T. Veel, O. Villanger, M.R. Holthe, F.S. Skjorten, M.G. Raeder, Intravenous bilirubin infusion causes vacuolization of the cytoplasm of hepatocytes and canalicular cholestasis, Acta Physiol. Scand. 143 (1991) 421–429.

[17] L. Weaver, A.R. Hamoud, D.E. Stec, T.D. Hinds, Biliverdin reductase and bilirubin in hepatic disease, Am. J. Physiol. Gastrointest. Liver Physiol. 314 (2018) G668–G676.

[18] C. Yu, X. Chai, L. Yu, S. Chen, S. Zeng, Identification of novel pregnane X receptor activators from traditional Chinese medicines, J. Ethnopharmacol. 136 (2011) 137–143.

[19] H. Zeng, D. Li, X. Qin, P. Chen, H. Tan, X. Zeng, X. Li, X. Fan, Y. Jiang, Y. Zhou, Y. Wang, M. Huang, Hepatoprotective Effects of Schisandra sphenanthera Extract against Lithocholic Acid-Induced Cholestasis in Male Mice Are Associated with Activation of the Pregnane X Receptor Pathway and Promotion of Liver Regeneration, Drug Metabolism Disposition: Biol. Fate Chem. 44 (2016) 337–342.

[20] X. Li, J. Sun, X. Fan, L. Guan, D. Li, Y. Zhou, X. Zeng, Y. Chen, H. Zhang, L. Xu, F. Jiang, M. Huang, H. Bi, Schisandrol B promotes liver regeneration after partial hepatectomy in mice, Eur. J. Pharmacol. 818 (2018) 96–102.

[21] M.I. Nasser, S. Zhu, C. Chen, M. Zhao, H. Huang, P. Zhu, A Comprehensive Review on Schisandrin B and Its Biological Properties, Oxid. Med. Cell. Longevity 2020 (2020) 2172740.

[22] J.N. Chun, S. Park, S. Lee, J.K. Kim, E.J. Park, M. Kang, H.K. Kim, J.K. Park, I. So, J. H. Jeon, Schisandrol B and schisandrin B inhibit TGFbeta1-mediated NF-kappaB activation via a Smad-independent mechanism, Oncotarget 9 (2018) 3121–3130.

[23] M. Zhu, T. Lu, Y. Jia, X. Luo, P. Gopal, L. Li, M. Odewole, V. Renteria, A.G. Singal, Y. Jang, K. Ge, S.C. Wang, M. Sorouri, J.R. Parekh, M.P. MacConmara, A.C. Yopp, T. Wang, H. Zhu, Somatic mutations increase hepatic clonal fitness and regeneration in chronic liver disease, Cell 177 (608–21) (2019), e12.

[24] J. Zhang, R. Li, Q. Liu, J. Zhou, H. Huang, Y. Huang, Z. Zhang, T. Wu, Q. Tang, C. Huang, Y. Zhao, G. Zhang, L. Mo, Y. Li, J. He, SB431542-Loaded Liposomes Alleviate Liver Fibrosis by Suppressing TGF-beta Signaling, Mol. Pharm. 17 (2020) 4152–4162.

[25] S. Wang, Y. Lin, Z. Zhou, L. Gao, Z. Yang, F. Li, B. Wu, Circadian clock gene bmal1 regulates bilirubin detoxification: A potential mechanism of feedback control of hyperbilirubinemia, Theranostics 9 (2019) 5122–5133.

[26] X. Gao, X. Yang, B. Zhang, Neuroprotection of taurine against bilirubin-induced elevation of apoptosis and intracellular free calcium ion in vivo, Toxicol. Mech. Methods 21 (2011) 383–387.

[27] P. Gou, X. Qi, R. Yuan, H. Li, X. Gao, J. Wang, B. Zhang, Tet1-mediated DNA demethylation involves in neuron damage induced by bilirubin in vitro, Toxicol. Mech. Methods 28 (2018) 55–61.

[28] Q. Yu, Z. Liao, D. Liu, W. Xie, Z. Liu, G. Liao, C.Y. Wang, Small molecule inhibitors of the prostate cancer target KMT2D, Biochem. Biophys. Res. Commun. 533 (2020) 540–547.

[29] B. Shah, G. Shah, Antifibrotic effect of heparin on liver fibrosis model in rats, World J. Gastrointestinal Pharmacol. Therapeut. 3 (2012) 86–92.

[30] O.A. Zargar, R. Bashir, S.A. Ganie, A. Masood, M.A. Zargar, R. Hamid, Hepatoprotective Potential of Elsholtzia densa Against Acute and Chronic Models of Liver Damage in Wistar Rats, Drug Res. 68 (2018) 567–575.

[31] M. Bhadauria, Propolis prevents hepatorenal injury induced by chronic exposure to carbon tetrachloride, Evidence-based complementary and alternative medicine : eCAM 2012 (2012), 235358.

[32] T. Luedde, R.F. Schwabe, NF-kappaB in the liver–linking injury, fibrosis and hepatocellular carcinoma, Nat. Rev. Gastroenterol. Hepatol. 8 (2011) 108–118.

[33] Y.H. Li, S.H. Woo, D.H. Choi, E.H. Cho, Succinate causes alpha-SMA production through GPR91 activation in hepatic stellate cells, Biochem. Biophys. Res. Commun. 463 (2015) 853–858.

[34] A.V. Shinde, C. Humeres, N.G. Frangogiannis, The role of alpha-smooth muscle actin in fibroblast-mediated matrix contraction and remodeling, Bba-Mol Basis Dis 1863 (2017) 298–309.

[35] Y. Makino, H. Hikita, T. Kodama, M. Shigekawa, R. Yamada, R. Sakamori, H. Eguchi, E. Morii, H. Yokoi, M. Mukoyama, S. Hiroshi, T. Tatsumi, T. Takehara, CTGF Mediates Tumor-Stroma Interactions between Hepatoma Cells and Hepatic Stellate Cells to Accelerate HCC Progression, Cancer Res. 78 (2018) 4902–4914.

[36] H.K. Seitz, F. Stickel, Risk factors and mechanisms of hepatocarcinogenesis with special emphasis on alcohol and oxidative stress, Biol. Chem. 387 (2006) 349–360.

[37] Y. Liu, H.Y. Yu, Y.M. Wang, T. Tian, W.M. Wu, M. Zhou, X.G. Meng, H.L. Ruan, Neuroprotective Lignans from the Fruits of Schisandra bicolor var. tuberculata, J. Nat. Prod. 80 (2017) 1117–1124.

[38] X.Y. Chen, R. Tang, T.T. Liu, W. Dai, Q. Liu, G.P. Gong, S. Song, M.H. Hu, L. J. Huang, Z.F. Wang, Physicochemical properties, antioxidant activity and immunological effects *in vitro* of polysaccharides from Schisandra sphenanthera and Schisandra chinensis, Int. J. Biol. Macromol. 131 (2019) 744–751.

[39] X. Li, X.M. Fan, D.S. Li, X.Z. Zeng, H. Zeng, Y.T. Wang, Y.W. Zhou, Y.X. Chen, M. Huang, H.C. Bi, Schisandra sphenanthera Extract Facilitates Liver Regeneration after Partial Hepatectomy in Mice, Drug Metab. Dispos. 44 (2016) 647–652.

[40] L.L. Lu, J. Zhou, J. Shi, X.J. Peng, X.X. Qi, Y. Wang, F.Y. Li, F.Y. Zhou, L. Liu, Z. Q. Liu, Drug-metabolizing activity, protein and gene expression of UDP-glucuronosyltransferases are significantly altered in hepatocellular carcinoma patients, PLoS One 10 (2015).

[41] P.Z. Li, K. He, J.Z. Li, Z.J. Liu, J.P. Gong, The role of Kupffer cells in hepatic diseases, Mol. Immunol. 85 (2017) 222–229.

[42] W.C. Peng, C.Y. Logan, M. Fish, T. Anbarchian, F. Aguisanda, A. Alvarez-Varela, P. Wu, Y. Jin, J. Zhu, B. Li, M. Grompe, B. Wang, R. Nusse, Inflammatory Cytokine TNFalpha Promotes the Long-Term Expansion of Primary Hepatocytes in 3D Culture, Cell 175 (1607–19) (2018), e15.

[43] T.Y. Shiu, T.Y. Huang, S.M. Huang, Y.L. Shih, H.C. Chu, W.K. Chang, T.Y. Hsieh, Nuclear factor kappaB down-regulates human UDP-glucuronosyltransferase 1A1: a novel mechanism involved in inflammation-associated hyperbilirubinaemia, Biochem. J. 449 (2013) 761–770.

[44] C. He, J. Feng, H. Huang, Z. Hua, Caspase-1 involves in bilirubin-induced injury of cultured rat cortical neurons, Pediatr. Res. 86 (2019) 492–499.

[45] O. Bulut, A. Erek, S. Duruyen, Effects of hyperbilirubinemia on markers of genotoxicity and total oxidant and antioxidant status in newborns, Drug Chem. Toxicol. (2020) 1–5.

[46] Rawat V, Bortolussi G, Gazzin S, Tiribelli C, Muro AF. Bilirubin-Induced Oxidative Stress Leads to DNA Damage in the Cerebellum of Hyperbilirubinemic Neonatal Mice and Activates DNA Double-Strand Break Repair Pathways in Human Cells. Oxidative medicine and cellular longevity 2018:1801243.

[47] S.F. Asad, S. Singh, A. Ahmad, S.M. Hadi, Bilirubin/biliverdin-Cu(II) induced DNA breakage; reaction mechanism and biological significance, Toxicol. Lett. 131 (2002) 181–189.

[48] Vianello E, Zampieri S, Marcuzzo T, Tordini F, Bottin C, Dardis A, Zanconati F, Tiribelli C, Gazzin S. Histone acetylation as a new mechanism for bilirubin-induced encephalopathy in the Gunn rat. Scientific reports 2018;8.

[49] Huang HB, Guo MX, Liu NN, Zhao C, Chen HY, Wang XL, Liao SY, Zhou P, Liao YN, Chen X, Lan XY, Chen JH, Xu DC, Li XF, Shi XP, Yu L, Nie, YQ, Wang XJ, Zhang CE, Liu JB. Bilirubin neurotoxicity is associated with proteasome inhibition. Cell death & disease 2017;8.

[50] G.H. Oakes, J.R. Bend, Early steps in bilirubin-mediated apoptosis in murine hepatoma (Hepa 1c1c7) cells are characterized by aryl hydrocarbon receptor-independent oxidative stress and activation of the mitochondrial pathway, J. Biochem. Mol. Toxicol. 19 (2005) 244–255.

[51] J.M. Seubert, A.J. Darmon, A.O. El-Kadi, S.J. D'Souza, J.R. Bend, Apoptosis in murine hepatoma hepa 1c1c7 wild-type, C12, and C4 cells mediated by bilirubin, Mol. Pharmacol. 62 (2002) 257–264.

[52] J. Sugatani, Function, genetic polymorphism, and transcriptional regulation of human UDP-glucuronosyltransferase (UGT) 1A1, Drug Metab. Pharmacokinet. 28 (2013) 83–92.

[53] C.Q. Ning, X.G. Gao, C.Y. Wang, Y.L. Kong, Z.H. Liu, H.J. Sun, P.Y. Sun, X.K. Huo, X.D. Ma, Q. Meng, K.X. Liu, Ginsenoside Rg1 protects against acetaminophen-induced liver injury via activating Nrf2 signaling pathway in vivo and in vitro, Regul Toxicol Pharm 98 (2018) 58–68.

[54] B.M. Shi, Y. Su, S.Y. Chang, Y.C. Sun, X.Y. Meng, A.S. Shan, Vitamin C protects piglet liver against zearalenone-induced oxidative stress by modulating expression of nuclear receptors PXR and CAR and their target genes, Food Funct. 8 (2017) 3675–3687.

[55] Li TT, Xu LJ, Zheng RY, Wang XJ, Li LW, Ji H, Hu QH. et al. Picroside II protects against cholestatic liver injury possibly through activation of farnesoid X receptor. Phytomedicine : international journal of phytotherapy and phytopharmacology 2020;68.

[56] R. Kundu, S. Dasgupta, A. Biswas, S. Bhattacharya, B.C. Pal, S. Bhattacharya, P. G. Rao, N.C. Barua, M. Bordoloi, S. Bhattacharya, Carlinoside reduces hepatic bilirubin accumulation by stimulating bilirubin-UGT activity through Nrf2 gene expression, Biochem. Pharmacol. 82 (2011) 1186–1197.

[57] S. Fan, C. Liu, Y. Jiang, Y. Gao, Y. Chen, K. Fu, X. Yao, M. Huang, H. Bi, Lignans from Schisandra sphenanthera protect against lithocholic acid-induced cholestasis by pregnane X receptor activation in mice, J. Ethnopharmacol. 245 (2019), 112103.